

An adaptive high order direct solution technique for elliptic boundary value problems

P. Geldermans and A. Gillman

Department of Computational and Applied Mathematics, Rice University

Abstract: This manuscript presents an adaptive high order discretization technique for elliptic boundary value problems. The technique is applied to an updated version of the Hierarchical Poincaré-Steklov (HPS) method. Roughly speaking, the HPS method is based on local pseudospectral discretizations glued together with Poincaré-Steklov operators. The new version uses a modified tensor product basis which is more efficient and stable than previous versions. The adaptive technique exploits the tensor product nature of the basis functions to create a criterion for determining which parts of the domain require additional refinement. The resulting discretization achieves the user prescribed accuracy and comes with an efficient direct solver. The direct solver increases the range of applicability to time dependent problems where the cost of solving elliptic problems previously limited the use of implicit time stepping schemes.

1. INTRODUCTION

This manuscript presents an adaptive discretization technique for problems of the form

$$(1) \quad \begin{cases} Au(\mathbf{x}) = g(\mathbf{x}) & \mathbf{x} \in \Omega, \\ u(\mathbf{x}) = f(\mathbf{x}) & \mathbf{x} \in \Gamma = \partial\Omega, \end{cases}$$

where Ω is a rectangle in \mathbb{R}^2 with boundary Γ , and where A is a coercive elliptic partial differential operator

$$(2) \quad [Au](\mathbf{x}) = -c_{11}(\mathbf{x})[\partial_1^2 u](\mathbf{x}) - 2c_{12}(\mathbf{x})[\partial_1 \partial_2 u](\mathbf{x}) - c_{22}(\mathbf{x})[\partial_2^2 u](\mathbf{x}) \\ + c_1(\mathbf{x})[\partial_1 u](\mathbf{x}) + c_2(\mathbf{x})[\partial_2 u](\mathbf{x}) + c(\mathbf{x})u(\mathbf{x}).$$

The discretization technique presented here is an updated version of the composite spectral discretization techniques presented in [18, 17, 23]. It is based on local pseudospectral discretizations that are “glued” together by Poincaré-Steklov operators. These Poincaré-Steklov operators are glued in a hierarchically yielding a direct solver. Hence, the discretization technique is called the Hierarchical Poincaré-Steklov (HPS) method. The adaptive refinement strategy presented in this manuscript is inspired by the technique in [21] which determines which parts of the geometry to refine by looking at Chebychev expansion coefficients of the local approximate solution. Like the HPS methods in [18, 17, 23, 1], the adaptive discretization technique can also be modified to handle a range of different domains, including curved ones. Additional novelty of this paper lies in an update to the local discretization. The new local discretization uses a modified tensor product basis which makes the local discretization less expensive than previous versions [18, 17, 23, 1] and the whole algorithm easier to implement.

While constructing the adaptive discretization and the direct solver has a computational cost that scales $O(N^{3/2})$ where N is the number of discretization points, the cost of applying the solver is $O(N \log N)$ with a small constant. The constant in the solve step is typically much smaller than for a uniform discretization thus making the method useful for applications that involve *many* elliptic solves that require locally refined high order discretizations. For example, having an efficient direct solver for elliptic partial differential equations can increase the range of problems for which implicit time stepping schemes are computationally affordable.

1.1. Overview of discretization technique. Roughly speaking the adaptive discretization technique can be broken into three steps.

- Step 1: First, the geometry is partitioned into a collection of patches using an quad tree with an adaptive interpolation strategy applied so that the coefficients in (2) and body load function $g(\mathbf{x})$ in (1) are captured to the user prescribed tolerance ϵ .
- Step 2: Next each patch is discretized using a high order spectral collocation technique and the patches are “glued” together at the boundaries via a Poincaré-Steklov operators in a hierarchical fashion. In the process of gluing patches together, solution operators that propagate boundary data to the interior of a box are constructed. Then by applying the solution operators (small matrix vector multiplies) the boundary data is propagated down the hierarchical tree giving an approximate solution on each patch.
- Step 3: All patches are checked to see if they need to be further refined. If there are patches marked for refinement, they are refined and steps 2 and 3 are repeated until no patches are marked for refinement. If the refinement is localized in the domain, the bulk of the computation from step 2 can be reused.

While the method can be employed with any Poincaré-Steklov operator, for simplicity of presentation, this paper uses the Dirichlet-to-Neumann operator for gluing boxes as in [18, 23, 1]. For the Helmholtz experiments in this paper, the impedance-to-impedance (ItI) operator is used instead. [17] presents the ItI version of the solution technique for a homogeneous PDE. The appendix of this manuscript presents the ItI based solution technique when there is a body load $g(\mathbf{x})$.

1.2. Applications utilizing the HPS method. While the HPS method is relatively new, it is already being utilized for scattering problems. Applications involving scattering problems include underwater acoustics [4], ultrasound and microwave tomography [14, 30], wave propagation in metamaterials and photonic crystals, and seismology [31]. In [17], the HPS method was extended to free space scattering problems where the deviation from a constant coefficient problem had compact support. The numerical results in that paper showed the method did not observe pollution for problems where the support of the deviation from constant coefficient was 100 time the smallest wavelength in size. In [5], the method was utilized to build a inverse scattering solver via the recursive linearization procedure proposed in [9]. The recursive linearization procedure requires solving a sequence of linear least squares problems at successively higher frequencies to reconstruct an unknown sound speed. Next, in [6], the HPS method was utilized for inverse scattering problems with a random noisy background medium. In each of these inverse scattering solvers, the least squares solve requires solving the same variable coefficient elliptic partial differential equation many times to apply the forward and adjoint operators. The proposed adaptive discretization could improve the efficiency of the techniques listed in this section.

1.3. Prior and related work. There is a vast literature of adaptive methods for finite element (FEM) based discretization techniques for elliptic problems. A high level overview is presented here. Early works [13, 2] focused on defining appropriate error estimators for Poisson problems using face and volume residuals giving the user the ability to identify where to refine. Recent trends in adaptive FEM for Poisson problems focus on proving that the adaptive algorithms converge [25, 8]. A local indicators and error estimators for FEM applied to Helmholtz problems are presented in [3]. There has also been an extensive work on hp-adaptivity [26, 10, 11]. The adaptive discretization presented here is an h-adaptive scheme which is specific for the HPS discretization technique. The local error indicator can be (and is) applied to both Poisson and Helmholtz problems. The relative convergence error stopping criterion determines if the problem has been resolved.

The direct solver for the HPS discretization is related to the direct solvers for sparse systems arising from finite difference and finite element discretizations of elliptic PDEs such as the classical nested dissection method of George [15, 19] and the multifrontal methods by Duff and others [12]. These methods can be viewed as a hierarchical version of the “static condensation” idea in finite element analysis [32]. High order finite difference and finite element discretizations lead to large frontal matrices (since the “dividers” that partition the grid have to be wide), and consequently

very high cost of the LU-factorization (see, e.g., Table 2 in [18]). It has been demonstrated that the dense matrices that arise in these solvers have internal structure that allows the direct solver to be accelerated to linear or close to linear complexity, see, e.g., [33, 16, 20, 22, 27]. The HPS discretization technique has one dimensional “dividers” independent of order and thus the direct solver only pays (in terms of computational complexity) the price of high order at the lowest level in the hierarchical tree. The same ideas that accelerate the nested dissection and multifrontal solvers can be applied the HPS direct solver [18].

In the previous versions of the HPS method special care was taken to deal with or avoid discretization points at the corners of the small patches. The method presented in [23] involves tedious bookkeeping of corner points. Additionally, possible singularities at the corners of the geometry Ω are of concern. By introducing interpolation at the level of the local discretizations, the methods in [18, 1, 17] avoid the corners of Ω . The new local discretization presented in this manuscript does not involve the corner points at all; thus improving the robustness and efficiency of the method.

1.4. Outline of paper. For simplicity of presentation, the proposed algorithm is described for a PDE with no body load (i.e. $g(\mathbf{x}) = 0$ in (1)). The manuscript begins by reviewing the HPS method with uniform refinement in section 2 but with the *new* local discretization technique. Next, the adaptive refinement procedure is presented in section 3. Then, numerical experiments demonstrating the performance of the method in section 4. Finally the manuscript concludes with a summary of the paper in section 5.

2. THE HPS METHOD

This section presents the HPS method with a new local discretization technique. The HPS method begins by partitioning the domain Ω into a collection of square (or possibly rectangular) boxes, called *leaf boxes*. Throughout this paper, we assume that the parameter for the order of the discretization n_c is fixed ($n_c = 16$ is often a good choice). For a uniform discretization, the size of all leaf boxes is chosen so that any potential u of equation (1), as well as its first and second derivatives, can be accurately interpolated from their values at the local discretization points on any leaf box.

Next a binary tree on the collection of leaf boxes is constructed by hierarchically merging them, making sure that all boxes on the same level are roughly of the same size, cf. Figure 1. The boxes should be ordered so that if τ is a parent of a box σ , then $\tau < \sigma$. We also assume that the root of the tree (i.e. the full box Ω) has index $\tau = 1$. We let Ω^τ denote the domain associated with box τ . If a box ρ is child of σ and σ is a child of τ , we call ρ a *grandchild* of τ . For example in Figure 1, boxes 16 – 19 are grandchildren of box 4. (This vocabulary is needed for the adaptive scheme presented in section 3.)

For each leaf box, approximate Dirichlet-to-Neumann (DtN) and solution operators are constructed via the *modified* spectral collocation method presented in section 2.1. The DtN approximations are “glued” together in a hierarchical fashion two boxes at a time. Section 2.2 presents the technique for constructing approximate DtN and solution operators for the union of two boxes. Algorithm 1 gives an overview of the construction of the discretization and direct solver. Once the hierarchical collection of approximate solution operators is constructed, the solution on the interior can be found for $O(N \log N)$ cost via Algorithm 2.

Definition 2.1 (Dirichlet-to-Neumann map). For domain Ω with boundary Γ , the Dirichlet-to-Neumann (DtN) operator $T : H^1(\Gamma) \rightarrow L^2(\Gamma)$ is defined by

$$(3) \quad Tf = u_n,$$

for any Dirichlet boundary data $f(x) \in H^1(\Gamma)$, where u_n denotes the normal derivative of u on Γ in the direction of the normal vector n pointing out of Ω .



FIGURE 1. The square domain Ω is split into 4×4 leaf boxes. These are then gathered into a binary tree of successively larger boxes as described in Section 2. One possible enumeration of the boxes in the tree is shown, but note that the only restriction is that if box τ is the parent of box σ , then $\tau < \sigma$.

2.1. Leaf computation. This section describes a modified spectral collocation method for constructing approximate DtN \mathbf{T}^τ and solution Ψ^τ operators for a leaf box τ .

The modified spectral collocation technique begins with the classic $n_c \times n_c$ product Chebychev grid and the corresponding differential matrices \mathbf{D}_x and \mathbf{D}_y from for example [29]. Let I_i^τ denote the index vector corresponding to points on the interior of Ω^τ and I_b^τ denote the index vector corresponding to points on the boundary of Ω^τ **not** including the corner points based on the tensor classic tensor grid. Figure 2 illustrates the indexing of the points in terms of the classic discretization. Thus $\{\mathbf{x}_j\}_{j=1}^{n_c^2-4}$ denotes the discretization points in Ω^τ given by the union of the red and blue points

in Figure 2. We order the solution vector \mathbf{u} and flux vector \mathbf{v} according to the following: $\mathbf{u} = \begin{bmatrix} \mathbf{u}_b \\ \mathbf{u}_i \end{bmatrix}$

where \mathbf{u}_b and \mathbf{u}_i denote the approximate values of the solution on the boundary and the interior, respectively. The ordering of the entries related to the boundary corresponding to the discretization points is $I_b^\tau = [I_s, I_e, I_n, I_w]$ where I_s denotes the blue points on the south boundary in Figure 2, etc. Let $I^\tau = [I_b^\tau, I_i^\tau]$ denote the collection of all indices that are used in the discretization.

Thanks to the tensor product basis, we know the entries of \mathbf{D}_x and \mathbf{D}_y corresponding to the interaction of the corner points with the points on the interior of Ω^τ are zero. The directional basis functions for the other points on the boundary are not impacted by the removal of the corner points. Thus the differential operators from the classic pseudospectral discretization can be used to create the approximation of the local differential operator and DtN.

The classic discrete approximation of the differential operator on Ω^τ is given by

$$\mathbf{A} = -\mathbf{C}_{11}\mathbf{D}_x^2 - 2\mathbf{C}_{12}\mathbf{D}_x\mathbf{D}_y - \mathbf{C}_{22}\mathbf{D}_y^2 + \mathbf{C}_1\mathbf{D}_x + \mathbf{C}_2\mathbf{D}_y + \mathbf{C},$$

where \mathbf{C}_{11} is the diagonal matrix with diagonal entries $\{c_{11}(\mathbf{x}_k)\}_{k=1}^{n_c^2}$, and the other matrices \mathbf{C}_{ij} , \mathbf{C}_i , \mathbf{C} are defined analogously. Then the discretized differential equation on the new set of discretization points is given by

$$\begin{bmatrix} \mathbf{I} & \mathbf{0} \\ \mathbf{A}_{i,b} & \mathbf{A}_{i,i} \end{bmatrix} \begin{bmatrix} \mathbf{u}_b \\ \mathbf{u}_i \end{bmatrix} = \begin{bmatrix} \hat{\mathbf{f}} \\ \mathbf{0} \end{bmatrix}$$

where $\mathbf{A}_{i,i} = \mathbf{A}(I_i^\tau, I_i^\tau)$ is a matrix of size $(n_c - 2)^2 \times (n_c - 2)^2$, $\mathbf{A}_{i,b} = \mathbf{A}(I_i^\tau, I_b^\tau)$ is a matrix of size $(n_c - 2)^2 \times (4n_c - 8)$, and $\hat{\mathbf{f}}$ is vector of length $4n_c - 8$ containing fictitious Dirichlet boundary data.

When the boundary data is known, the approximate solution at the interior points is given by

$$(4) \quad \mathbf{u}_i = -\mathbf{A}_{i,i}^{-1}\mathbf{A}_{i,b}\mathbf{u}_b = \Psi^\tau\mathbf{u}_b$$

where the matrix Ψ^τ is the approximate solution operator. Since the matrix $\mathbf{A}_{i,i}$ is not large (even for $n_c = 16$), it can be inverted quickly using dense linear algebra.

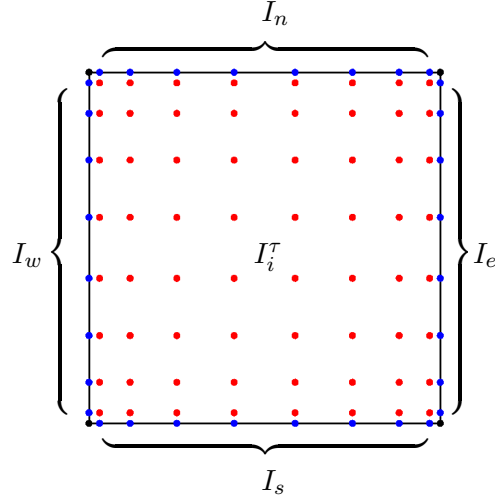


FIGURE 2. Illustration of the discretization points for a leaf box τ . The points in blue are the boundary points with indices $I_b^\tau = [I_s, I_e, I_n, I_w]$. The points in red are the interior points with indices I_i^τ . The points in black are the omitted corner points.

Let \mathbf{L} denote the matrix made up of four block row matrices corresponding to taking the normal derivative of the basis functions on the leaf τ along each of the edges. In terms of the discrete operators \mathbf{L} is given by

$$\mathbf{L} = \begin{bmatrix} \mathbf{D}_x(I_s, I^\tau) \\ \mathbf{D}_y(I_e, I^\tau) \\ \mathbf{D}_x(I_n, I^\tau) \\ \mathbf{D}_y(I_w, I^\tau) \end{bmatrix}.$$

To construct the approximate DtN operator \mathbf{T}^τ , we take the normal derivative of the solution by applying \mathbf{L} to $\begin{bmatrix} \mathbf{I}_{4n_c-8} \\ \boldsymbol{\Psi}^\tau \end{bmatrix}$, i.e.

$$\mathbf{T}^\tau = \mathbf{L} \begin{bmatrix} \mathbf{I}_{4n_c-8} \\ \boldsymbol{\Psi}^\tau \end{bmatrix}$$

where \mathbf{I}_{4n_c-8} denotes the identity matrix of size $4n_c - 8$.

Remark 1. The classic tensor product discretization can be used to formulate the new discretization thanks to the separable basis (i.e. the corner points do not contribute the discretized differential equation). While interpolation along the edges without the corners is less accurate than if the corners were included, it is stable [28]. Since the discretization is run at high order (typically $n_c \geq 16$), a loss in accuracy is not observed in practice.

2.2. Merging two boxes. This section reviews of the procedure for constructing the DtN and solution matrices for the union of two boxes for which DtN matrices have already been constructed. More detailed descriptions are presented in [18, 23, 1].

Let Ω^τ denote a box with children Ω^α and Ω^β so that

$$\Omega^\tau = \Omega^\alpha \cup \Omega^\beta.$$

For concreteness, let us assume that Ω^α and Ω^β share a vertical edge as shown in Figure 3. We partition the points on $\partial\Omega^\alpha$ and $\partial\Omega^\beta$ into three sets:

- I_1 Boundary nodes of Ω^α that are not boundary nodes of Ω^β .
- I_2 Boundary nodes of Ω^β that are not boundary nodes of Ω^α .
- I_3 Boundary nodes of both Ω^α and Ω^β that are *not* boundary nodes of the union box Ω^τ .

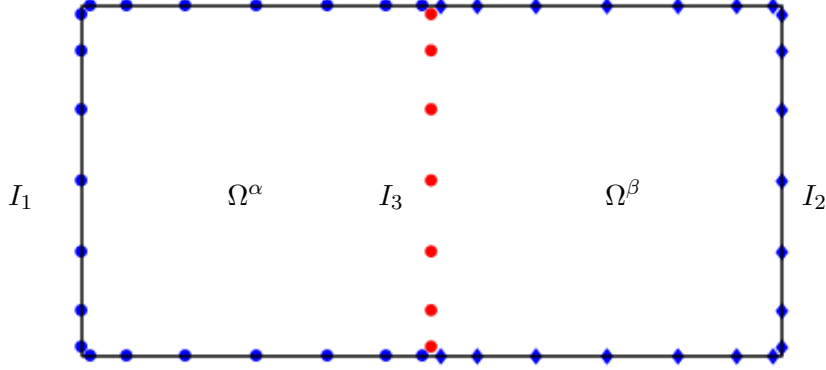


FIGURE 3. Notation for the merge operation described in Section 2.2. The rectangular domain Ω is formed by two squares Ω^α and Ω^β . The sets I_1 (blue circles) and I_2 (blue diamonds) form the exterior nodes, while I_3 (red circles) consists of the interior nodes.

The indexing for the points on the interior and boundary of Ω^τ are $I_1^\tau = I_3$ and $I_b^\tau = [I_1, I_2]$, respectively.

Let u denote a solution to (1), with tabulated potential values \mathbf{u} and boundary fluxes \mathbf{v} . Ordering the DtN operators according to the I_k defined in Figure 3 results in the equations

$$(5) \quad \begin{bmatrix} \mathbf{v}_1 \\ \mathbf{v}_3 \end{bmatrix} = \begin{bmatrix} \mathbf{T}_{1,1}^\alpha & \mathbf{T}_{1,3}^\alpha \\ \mathbf{T}_{3,1}^\alpha & \mathbf{T}_{3,3}^\alpha \end{bmatrix} \begin{bmatrix} \mathbf{u}_1 \\ \mathbf{u}_3 \end{bmatrix}, \quad \text{and} \quad \begin{bmatrix} \mathbf{v}_2 \\ \mathbf{v}_3 \end{bmatrix} = \begin{bmatrix} \mathbf{T}_{2,2}^\beta & \mathbf{T}_{2,3}^\beta \\ \mathbf{T}_{3,2}^\beta & \mathbf{T}_{3,3}^\beta \end{bmatrix} \begin{bmatrix} \mathbf{u}_2 \\ \mathbf{u}_3 \end{bmatrix}$$

where $\mathbf{T}_{1,1}^\alpha = \mathbf{T}^\alpha(I_1, I_1)$, etc. Noting that \mathbf{v}_3 and the solution \mathbf{u}_3 is the same for each box (since the solution is smooth), the solution operator Ψ^τ is found by equating the bottom two row equations of (5);

$$(6) \quad \mathbf{u}_3 = (\mathbf{T}_{3,3}^\alpha - \mathbf{T}_{3,3}^\beta)^{-1} [-\mathbf{T}_{3,1}^\alpha \mid \mathbf{T}_{3,2}^\beta] \begin{bmatrix} \mathbf{u}_1 \\ \mathbf{u}_2 \end{bmatrix} = \Psi^\tau \begin{bmatrix} \mathbf{u}_1 \\ \mathbf{u}_2 \end{bmatrix}.$$

The operator Ψ^τ in (6) maps the solution on the boundary of Ω^τ to the solution \mathbf{u}_3 on the interior edge. The DtN operator is then constructed by plugging equation (6) into the top row equations in (5) and combining them to a matrix equation. The result is

$$(7) \quad \begin{bmatrix} \mathbf{v}_1 \\ \mathbf{v}_2 \end{bmatrix} = \mathbf{T}^\tau \begin{bmatrix} \mathbf{u}_1 \\ \mathbf{u}_2 \end{bmatrix}$$

where

$$(8) \quad \mathbf{T}^\tau = \begin{bmatrix} \mathbf{T}_{1,1}^\alpha & \mathbf{0} \\ \mathbf{0} & \mathbf{T}_{2,2}^\beta \end{bmatrix} + \begin{bmatrix} \mathbf{T}_{1,3}^\alpha \\ \mathbf{T}_{2,3}^\beta \end{bmatrix} (\mathbf{T}_{3,3}^\alpha - \mathbf{T}_{3,3}^\beta)^{-1} [-\mathbf{T}_{3,1}^\alpha \mid \mathbf{T}_{3,2}^\beta].$$

3. ADAPTIVE DISCRETIZATION

This section presents an adaptive discretization technique for the boundary value problem (1) where the coefficient functions, right hand side and boundary data are smooth functions. As with the uniform discretization technique, the adaptive method produces a direct solver. The approximate solution obtained from the adaptive procedure is accurate (in the relative error) to a user prescribed tolerance ϵ .

At a high level, the idea stems from the fact that the discretization on a leaf can be accurate enough to capture the solution locally if it was given correct boundary data. The indicator for further refinement we propose in this section determines if the local basis is good enough to capture

ALGORITHM 1 (build solution operators)

This algorithm builds the global Dirichlet-to-Neumann operator for (1). It also builds all the solution matrices Ψ^τ required for constructing an approximation to u at any interior point.

It is assumed that if node τ is a parent of node σ , then $\tau < \sigma$.

-
- (1) **for** $\tau = N_{\text{boxes}}, N_{\text{boxes}} - 1, N_{\text{boxes}} - 2, \dots, 1$
 - (2) **if** (τ is a leaf)
 - (3) Construct \mathbf{T}^τ and Ψ^τ via the process described in Section 2.1.
 - (4) **else**
 - (5) Let σ_1 and σ_2 be the children of τ .
 - (6) Split $I_b^{\sigma_1}$ and $I_b^{\sigma_2}$ into vectors I_1, I_2 , and I_3 as shown in Figure 3.
 - (7) $\Psi^\tau = (\mathbf{T}_{3,3}^{\sigma_1} - \mathbf{T}_{3,3}^{\sigma_2})^{-1} [-\mathbf{T}_{3,1}^{\sigma_1} \mid \mathbf{T}_{3,2}^{\sigma_2}]$
 - (8) $\mathbf{T}^\tau = \begin{bmatrix} \mathbf{T}_{1,1}^{\sigma_1} & \mathbf{0} \\ \mathbf{0} & \mathbf{T}_{2,2}^{\sigma_2} \end{bmatrix} + \begin{bmatrix} \mathbf{T}_{1,3}^{\sigma_1} \\ \mathbf{T}_{2,3}^{\sigma_2} \end{bmatrix} \Psi^\tau.$
 - (9) Delete \mathbf{T}^{σ_1} and \mathbf{T}^{σ_2} .
 - (10) **end if**
 - (11) **end for**

ALGORITHM 2 (solve BVP once solution operator has been built)

This program constructs an approximation \mathbf{u} to the solution u of (1). It assumes that all matrices Ψ^τ have already been constructed in a pre-computation.

-
- (1) $\mathbf{u}(k) = f(\mathbf{x}_k)$ for all $k \in I_b^1$.
 - (2) **for** $\tau = 1, 2, 3, \dots, N_{\text{boxes}}$
 - (3) $\mathbf{u}(I_i^\tau) = \Psi^\tau \mathbf{u}(I_b^\tau).$
 - (4) **end for**

the solution locally. The stopping criterion for the adaptive procedure is based on the relative convergence error. This ensures that each leaf is given accurate boundary data. Starting such an adaptive technique with a global discretization of Ω would be computationally prohibitive. Instead, we initialize the mesh by utilizing the fact that the basis on a leaf should be able to represent the coefficient functions and the right hand side in (1) to the user prescribed ϵ .

Remark 2. In practice, one could likely get away with asking for less accuracy of the adaptive interpolation scheme. Since the interpolation is inexpensive compared to the cost of building the discretization and direct solver, we choose to be cautious.

The algorithm can be broken into seven steps.

Step 1: Use the adaptive interpolation technique from section 3.1 applied to the coefficient functions and the right hand side of equation (1). This yields an initial mesh.

Step 2: Construct an HPS solver for the non-uniform mesh resulting from the adaptive interpolation scheme via the techniques presented in section 3.2.

Let $\mathbf{u}^{\tau, \text{old}}$ denote the approximate solution on leaf box τ .

Step 3: Use indicator presented in section 3.3 to determine which boxes need additional refinement.

Step 4: If a leaf box τ has been marked for refinement, split into into four boxes ($\alpha_1, \alpha_2, \alpha_3$ and α_4).

Step 5: Discretize the new leaf boxes and update the direct solver. Since the discretization is localized and the direct solver is naturally domain decomposing, the direct solver can efficiently be updated without touching the entire geometry (see section 3.4).

Let $\mathbf{u}^{\tau,\text{new}}$ denote the solution on leaf box τ obtained with the new mesh.

Step 6: Check the relative convergence error by sweeping over all the leaf boxes on the old tree.

If leaf box τ was not refined, the relative convergence error for that box is defined to be

$$E_{\text{rel}}^{\tau} = \frac{\|\mathbf{u}^{\tau,\text{old}} - \mathbf{u}^{\tau,\text{new}}\|_2}{\|\mathbf{u}^{\tau,\text{old}} + \mathbf{u}^{\tau,\text{new}}\|_2}.$$

If leaf box τ was refined with grandchildren $\alpha_1, \alpha_2, \alpha_3$ and α_4 then the relative convergence error is defined as

$$E_{\text{rel}}^{\tau} = \frac{\|\mathbf{u}^{\tau,\text{old}} - \mathbf{L}\mathbf{u}_{\text{fine}}^{\tau}\|_2}{\|\mathbf{u}^{\tau,\text{old}} + \mathbf{L}\mathbf{u}_{\text{fine}}^{\tau}\|_2}$$

where $\mathbf{u}_{\text{fine}}^{\tau} = \begin{bmatrix} \mathbf{u}^{\alpha_1,\text{new}} \\ \mathbf{u}^{\alpha_2,\text{new}} \\ \mathbf{u}^{\alpha_3,\text{new}} \\ \mathbf{u}^{\alpha_4,\text{new}} \end{bmatrix}$, and \mathbf{L} is a matrix that interpolates functions from the fine discretization points to the coarse discretization points.

Step 7: If the average relative $E_{\text{rel}} = \frac{1}{n_{\tau}} \sum_{\tau} E_{\text{rel}}^{\tau} > \epsilon$ where τ is a leaf box on the old tree and n_{τ} is the number of leaf boxes in the old tree, the algorithm terminates. Otherwise, the vectors $\mathbf{u}^{\tau,\text{new}}$ get the label **old** and return to Step 3.

3.1. Adaptive interpolation. In order to keep the cost of the adaptive discretization as low as possible, we first create a mesh which allows for the smooth functions in (1) to be approximated with the local bases to the user prescribed tolerance ϵ . For simplicity of presentation, we describe the technique for interpolating a general smooth function $f(\mathbf{x})$ on Ω .

First, given n_c , a tensor product grid of n_c^2 Chebychev points is placed on Ω and each of its four grandchildren boxes (boxes 4, 5, 6 and 7 in Figure 1). Let $X^{\Omega} = \{\mathbf{x}_l^{\Omega}\}_{l=1}^{n_c^2}$ denote the set of interpolation points defined on box Ω . Likewise, let $X^j = \{\mathbf{x}_l^j\}_{l=1}^{n_c^2}$ for $j = 4, 5, 6,$ and 7 denote the set of interpolation points in box j . Set $X^{\text{grand}} = \bigcup_{j=4}^7 X^j$. Figure 4 illustrates the interpolation points on Ω and the four grandchildren when $n_c = 16$ and $\Omega = [0, 1]^2$.

Let \mathbf{f}^{Ω} denote the vector whose entries correspond to $f(\mathbf{x})$ evaluated at the points in X^{Ω} and \mathbf{L}_{etk} denote the interpolation operator which maps data from X^{Ω} to X^{grand} . (The notation etk stands for “elder to kids.”) Then $\mathbf{f}_{\text{app}} = \mathbf{L}_{\text{etk}}\mathbf{f}^{\Omega}$ is the approximate value of $f(\mathbf{x})$ at the points in X^{grand} interpolated from the values of $f(\mathbf{x})$ at the points in X^{Ω} . Let \mathbf{f}_{kids} denote the vector whose entries correspond to $f(\mathbf{x})$ evaluated at the points in X^{grand} . Let

$$E_{\text{interp}} = \frac{\|\mathbf{f}_{\text{kids}} - \mathbf{f}_{\text{app}}\|_2}{\|\mathbf{f}_{\text{kids}}\|_2}$$

denote the *relative interpolation error*. If $E_{\text{interp}} > \epsilon$, Ω is split into the four grandchildren boxes. The process is repeated for each of these smaller boxes. The process terminates when $E_{\text{interp}} \leq \epsilon$.

3.2. Non-uniform HPS solver. The mesh that results from the adaptive interpolation scheme is likely to be highly non-uniform. While the leaf level operations of the HPS method can remain the same as for the uniform mesh, the merge operation needs to be modified. Specifically, the boundary operators on the shared interface I_3 in Figure 6 need to “align.” We chose to align the operator via interpolation.

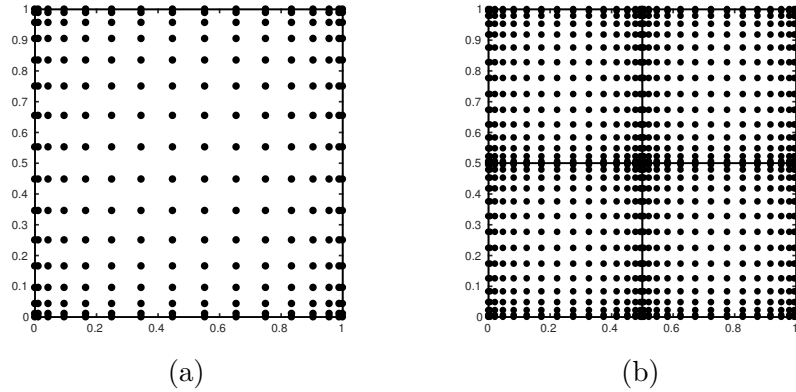


FIGURE 4. Illustration of the interpolation points on (a) $\Omega = [0, 1]^2$ and (b) its four grandchildren.

Interpolating a super fine mesh to a coarse mesh can be unstable. One approach to avoid stability problems is to use nested interpolation operators that recursively map two panels worth of interpolation points to one panels worth of interpolation points. Alternatively, a level restricted tree which requires all neighboring boxes be no more than two times bigger than each other is also stable. For two dimensional problems, we found the constant pre-factors favorable toward the latter approach. For three dimensional problems, the nested interpolation will likely be more efficient. Figure 5 illustrates the mesh resulting from the adaptive interpolation scheme with and without level restriction.

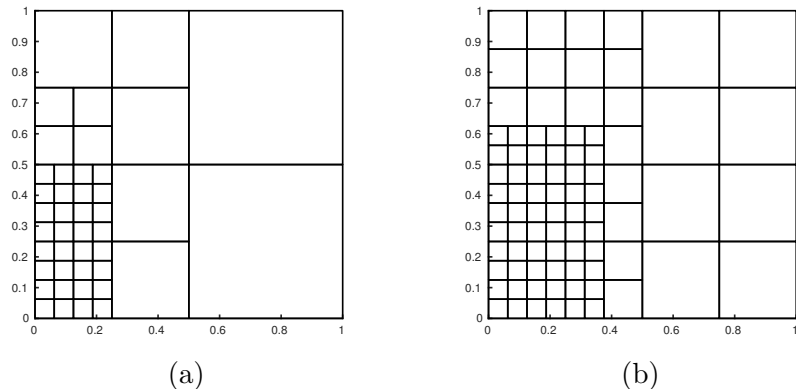


FIGURE 5. Illustration of the mesh resulting from adaptive interpolation applied to $f(\mathbf{x}) = f(x, y) = e^{-(1000(x-0.11)^2+100(y-0.27)^2)}$ (a) without and (b) with level restriction. The tolerance was set to $\epsilon = 1e - 6$ and $n_c = 16$.

The process of merging two boxes on different levels is straight forward. For simplicity of presentation, we present the technique for merging a leaf box α with a box β whose grandchildren are leaf boxes. In this situation, Ω^β has twice as many points on its boundary as Ω^α . Likewise, the DtN matrix \mathbf{T}^β is twice the size of \mathbf{T}^α . Figure 6 illustrates discretization points on the two boxes. The points in I_3 from box α do not match the points in I_3 from box β . In order to merge the two boxes, we use interpolation. Let \mathbf{L}_{2t1} and \mathbf{L}_{1t2} denote the interpolation operators that map two panels to one panel on the same interval and vice versa. Since there are $n_c - 2$ points on each panel, the interpolation operators are $n_c - 3$ order. Then the solution and DtN matrices on $\Omega^\tau = \Omega^\alpha \cup \Omega^\beta$ are given by inserting the interpolation operators into the appropriate locations in equations (6) and

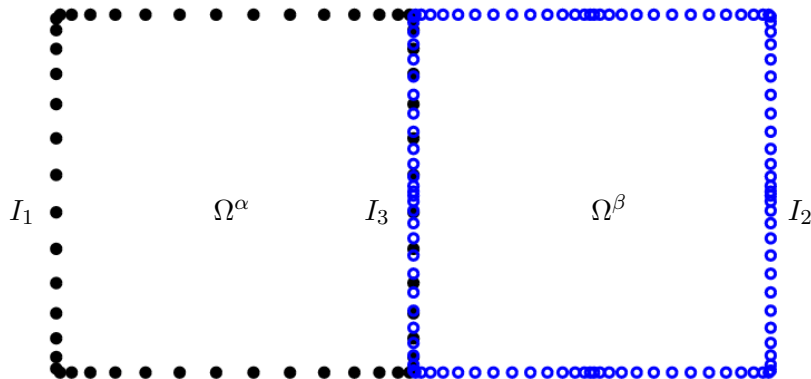


FIGURE 6. Notation for the merge operation when boxes are on different levels as described in Section 3.2. The rectangular domain Ω is formed by two squares Ω^α and Ω^β . The points on the boundary of Ω^α are solid black dots while the points on the boundary of the children of Ω^β are blue hollow dots.

(7);

$$\Psi^\tau = (\mathbf{T}_{3,3}^\alpha - \mathbf{L}_{2t1} \mathbf{T}_{3,3}^\beta \mathbf{L}_{1t2})^{-1} [-\mathbf{T}_{3,1}^\alpha \mid \mathbf{L}_{2t1} \mathbf{T}_{3,2}^\beta]$$

and

$$\mathbf{T}^\tau = \begin{bmatrix} \mathbf{T}_{1,1}^\alpha & \mathbf{0} \\ \mathbf{0} & \mathbf{T}_{2,2}^\beta \end{bmatrix} + \begin{bmatrix} \mathbf{T}_{1,3}^\alpha \\ \mathbf{T}_{2,3}^\beta \mathbf{L}_{1t2} \end{bmatrix} \Psi^\tau.$$

Remark 3. Merging two boxes on different levels was also presented in [1]. There the DtN operator \mathbf{T}^β is interpolated to a corresponding operator so that the number of points per edge matches the operator on box α . The method presented in this paper does not take this approach since the coarse sampling of boundary data on $\Omega^1 = \Omega$ may not be sufficient resulting in a loss of accuracy.

3.3. Indicator for refinement. This section presents a technique for identifying which leaf boxes need further refinement. The technique utilizes the fact that the local problem can be fully resolved even though the error is large due to incorrect boundary data. To determine if the local problem is fully resolved, the method we propose looks at the tail coefficients of the approximate solution written in a Chebychev expansion on the leaf boxes. This technique is inspired by [21] where a decay condition on the local Chebychev expansion coefficients was used to build an adaptive discretization technique for one dimensional integral equations.

Since each leaf box has a modified tensor product basis, the approximate solution u_{app} at any discretization point can be written as the product of two Lagrange polynomials $\Phi(x)$ and $\Psi(y)$ with x and y interpolation nodes respectively. Thus we will look at the *directional* Chebychev coefficients to build a refinement criterion. Recall that for one dimensional interpolation the Lagrange interpolant through Chebychev points can be expressed as a partial Chebychev expansion with coefficients that can be found via the Fast Fourier Transform (FFT)[7]. If the basis is sufficient to capture the solution locally, the series will be convergent and thus we can approximate the contributions from the remainder of the series by looking at the last few coefficients of the local expansions [21].

Specifically, for a leaf box Ω^τ , let $\{x_j\}_{j=1}^{n_c}$ and $\{y_j\}_{j=1}^{n_c}$ denote the one dimensional Chebychev interpolation points that the x and y coordinates of any discretization point. For a fixed x_j , $j = 2, \dots, n_c - 1$, let the vector \mathbf{B}_j of length n_c denote the Chebychev coefficients in the y -direction of the approximate solution along the line $x = x_j$ for $y \in [y_1, y_n]$; i.e. the entries in \mathbf{B}_j correspond to the coefficients of $\Psi(y)$ written in terms of Chebychev polynomials along the line $x = x_j$ in Ω^τ .

We define

$$S_y = \max_{j=2,\dots,n_c-1} (|\mathbf{B}_j(n_c - 1)| + |\mathbf{B}_j(n_c) - \mathbf{B}_j(n_c - 2)|)$$

be the indicator of the decay of the coefficients in the y -direction. Likewise for a fixed y_j , $j = 2, \dots, n_c - 1$, let \mathbf{C}_j denote vector of length n_c containing the Chebychev coefficients of the approximate solution along the line $y = y_j$ in Ω_τ (i.e. the x -direction coefficients) and define

$$S_x = \max_{j=2,\dots,n_c-1} (|\mathbf{C}_j(n_c - 1)| + |\mathbf{C}_j(n_c) - \mathbf{C}_j(n_c - 2)|)$$

to be the indicator of the decay of the coefficients in the x -direction. Then, for each leaf box τ , we define $S_\tau = \max\{S_x, S_y\}$. This yields a measure for how well the local basis is able capture solutions to the partial differential equation restricted to Ω^τ . Let

$$S_{\text{div}} = \frac{1}{4} \max_{\text{leaf boxes } \tau} S_\tau.$$

This gives a measure for how accurate we should hope the tail of the local expansions should be. Any leaf box that does not meet this requirement, i.e. $S_\tau > S_{\text{div}}$, is marked for further refinement. Algorithm 3 presents a pseudocode for determining which leaf boxes need refinement.

ALGORITHM 3 (Refinement indicator)

This algorithm presents the technique for determining which leaf boxes need additional refinement. It assumes a tree structured mesh and the corresponding direct solver are given.

-
- (1) **for** $\tau = N_{\text{boxes}}, N_{\text{boxes}} - 1, N_{\text{boxes}} - 2, \dots, 1$
 - (2) **if** (τ is a leaf)
 - (3) **for** $j = 2, \dots, n_c - 1$
 - (4) Compute the y -directional Chebychev coefficients \mathbf{B}_j of the approximate solution on τ .
 - (5) **end for**
 - (6) Let $S_y = \max_{j=2,\dots,n_c-1} (|\mathbf{B}_j(n_c - 1)| + |\mathbf{B}_j(n_c) - \mathbf{B}_j(n_c - 2)|)$
 - (7) **for** $j = 2, \dots, n_c - 1$
 - (8) Compute the x -directional Chebychev coefficients \mathbf{C}_j of the approximate solution on τ .
 - (9) **end for**
 - (10) Let $S_x = \max_{j=2,\dots,n_c-1} (|\mathbf{C}_j(n_c - 1)| + |\mathbf{C}_j(n_c) - \mathbf{C}_j(n_c - 2)|)$
 - (11) Let $S_\tau = \max\{S_x, S_y\}$
 - (12) **end if**
 - (13) **end for**
 - (14) Let $S_{\text{div}} = \frac{1}{4} \left(\max_{\text{leaf boxes } \tau} S_\tau \right)$.
 - (15) **for** $\tau = N_{\text{boxes}}, N_{\text{boxes}} - 1, N_{\text{boxes}} - 2, \dots, 1$
 - (16) **if** (τ is a leaf)
 - (17) **if** $S_\tau > S_{\text{div}}$
 - (18) Add τ to the refinement list.
 - (19) **end if**
 - (20) **end for**

3.4. Updating the solver. Once the list of leaf boxes marked for refinement is made, we need to solve (1) with the refined grid to determine if the mesh gives the desired accuracy. Constructing the direct solver from scratch is computationally expensive and unnecessary when the refinement is localized. This section presents a technique for building the solver for the refined mesh while making use of the existing solver. The key observation is the fact that the solution technique is naturally domain decomposing. This means that the only parts of the solver that need to be modified are the parts that touch the refined regions.

The first step in this process is to make a list of all boxes affected by the local refinement. To do this, starting from the list of boxes refined, we sweep the binary tree making note of all the ancestors affected. For example, if boxes 16, and 18 were the only boxes marked for refinement in Figure 1, the solver would need to update the operators for boxes 1, 2, 4, 8 and 9. The operators for the other boxes need not be touched.

Next DtN and solution matrices are constructed by moving through the list of effected boxes starting from the bottom of the tree (i.e. first processing the leaf boxes then its ancestors in order of ancestry).

Remark 4. Further acceleration can be gained by creating new tree structures based on the refinement regions. For the example where boxes 16 and 18 in Figure 1 require refinement, DtN and solution matrices can be constructed for the union of boxes 5, 6, 7, 17 and 19. Then the computation is limited to the boxes 16, 18, their union and gluing the union with the remainder of the geometry. For the problems under consideration in this manuscript, this technique was not employed.

4. NUMERICAL RESULTS

This section illustrates the ability of the adaptive discretization technique to solve a collection of problems. First, in section 4.1, three problems suggested in [24] to test adaptive discretization techniques for elliptic PDEs are considered. For each of these problems the solution is known but each poses a different challenge for adaptive discretization techniques. Section 4.2 considers two Helmholtz problems: a low- to mid-frequency constant coefficient problem with a source and a high frequency variable coefficient problem. The globally oscillatory nature of the solution adds to the challenge of accurately discretizing these problems.

The following quantities are reported.

n_c : the choice of discretization order

N_i : the number of leaf boxes after adaptive interpolation

N_f : the number of leaf boxes after adaptive discretization

T_i : the time in seconds for the adaptive interpolation step

T_f : the time in seconds for the adaptive discretization step

T_s : the time in seconds to apply the resulting solver

R : the memory in GB for storing the direct solver

For all experiments, the uniform discretization technique is applied for comparison purposes. T_{pre} is used to report the time in seconds for discretizing the PDE and building the direct solver.

To report on the accuracy of the solution techniques, we report

$$E_{\text{rel}} = \frac{1}{N_f} \sum_{\text{leaf boxes } \tau} E_{\text{rel}}^\tau$$

where

$$E_{\text{rel}}^\tau = \frac{\|\mathbf{u}_{\text{app}}^\tau - \mathbf{u}_{\text{ref}}^\tau\|_2}{\|\mathbf{u}_{\text{ref}}^\tau\|_2}$$

for leaf box τ , $\mathbf{u}_{\text{app}}^\tau$ is the approximate solution at the discretization points on τ , and $\mathbf{u}_{\text{ref}}^\tau$ is the reference solution evaluated at the discretization points on τ . For the problems where the solution is known, the reference solution is the exact solution. For problems where the solution is unknown,

the reference solution is given by an approximate solution obtained by running the uniform HPS method until convergence.

4.1. Problems with known solutions. This section reports the performance of the solution techniques for three problems where the solution is known and the partial differential equation has smooth coefficients on the domain $\Omega = (0, 1)^2$. The problems under consideration are the following:

Boundary layer: The Dirichlet boundary value problem

$$-\alpha \nabla^2 u + 2 \frac{\partial u}{\partial x} + \frac{\partial u}{\partial y} = f(x, y),$$

where the solution is given by

$$u(x, y) = (1 - e^{-(1-x)/\alpha})(1 - e^{-(1-y)/\alpha}) \cos(\pi(x + y))$$

and the parameter $\alpha = 10^{-3}$ determines the steepness of the boundary layer.

Locally oscillatory solution: The Dirichlet boundary value problem

$$-\nabla^2 u - \frac{1}{(\alpha + \sqrt{x^2 + y^2})^4} u = f(x, y),$$

where the solution is given by

$$u(x, y) = \sin \left(\frac{1}{\alpha + \sqrt{x^2 + y^2}} \right)$$

and the parameter $\alpha = \frac{1}{10\pi}$ determines the number of oscillations in the solution. The oscillations are clustered near the origin.

Wave front: The Poisson Dirichlet boundary value problem where the solution is given by

$$u(x, y) = \tan^{-1}(50(\sqrt{(x + 0.05)^2 + (y + 0.05)^2} - 0.7)).$$

Figure 7 illustrates the solutions to each of these problems. Table 1 reports the performance of the method for each of these problems with the stopping tolerance set to $\epsilon = 10^{-5}$ and different discretization orders $n_c = 8, 16$ and 32 . For all of the experiments the adaptive algorithm achieves the desired tolerance. In fact, for most of the experiments the discretization technique achieves better than the desired tolerance. The results also indicate that since the solutions to the boundary layer and locally oscillatory problem are “nicer” than the coefficients of the partial differential equation, the mesh achieved via the adaptive interpolation technique is more than sufficient for resolving the problem. For the wave front problem discretized with the low order basis, the adaptive discretization technique is needed to achieve the user specified tolerance. For all the experiments, it is computationally beneficial (less expensive to achieve the same or better accuracy) to use a higher order discretization. The timing results re-enforce the benefit of using the high order basis.

Figure 8 illustrates the mesh overlaid on the solution for each experiment. The mesh shows that the method is finding the areas where refinement is necessary. The denseness of the leaf boxes visualize the additional cost of using a low order method.

Tables 2-4 report the time in seconds for applying the uniform discretization technique to the three partial differential equations T_f and applying the direct solver T_s for different orders of discretization n_c and numbers of leaf boxes N_f . The memory R for storing the direct solver and the relative error E_{rel} are also reported. The cost for building the direct solver is more expensive for the adaptive discretization technique than for the uniform discretization. This is the case for most adaptive discretization techniques. The cost of applying the direct solver from the adaptive discretization is less expensive than applying the solver from the uniform discretization. To achieve the same accuracy as the adaptive discretization, the uniform discretization requires more leaf boxes and is more expensive (measured by adding the cost testing the finer grids).

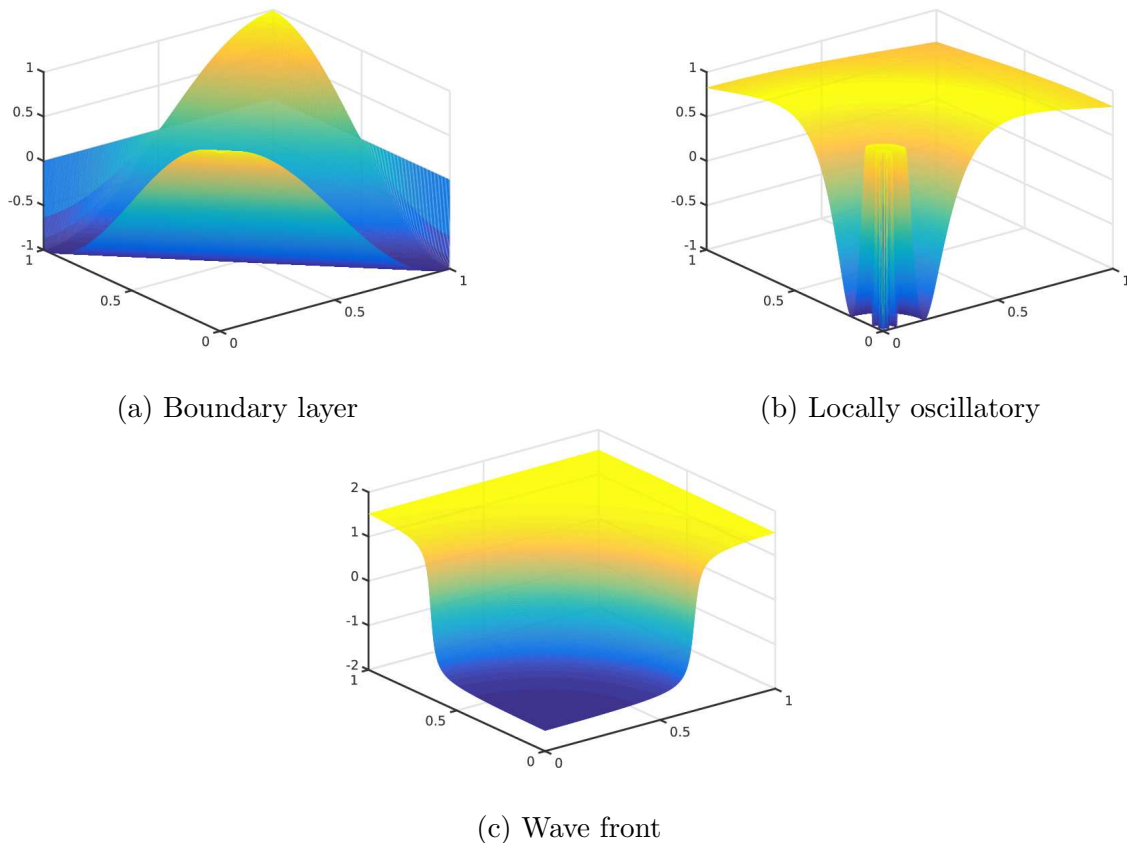


FIGURE 7. Illustration of the solutions to the problems under consideration in section 4.1: (a) Boundary layer problem, (b) Problem with a locally oscillatory solution, and (c) Problem where the solution is a wavefront.

Problem	n_c	N_i	N_f	T_i	T_f	T_s	R	E_{rel}
Boundary layer	8	66610	66610	3.58e+03	1.99e+02	1.01e+01	33.4	5.39e-09
	16	2194	2194	1.60e+01	3.18e+01	1.29e+00	2.99	7.27e-10
	32	316	316	2.42e+01	5.70e+01	4.97e-01	3.46	3.52e-13
Locally oscillatory	8	21247	21247	5.08e+02	4.24e+01	3.18e+00	5.57	1.35e-08
	16	487	487	4.43e+00	5.97e+00	2.21e-01	0.78	1.93e-08
	32	232	232	7.05e+00	2.14e+01	3.06e-01	3.15	4.06e-09
Wave front	8	44392	148087	1.28e+03	7.24e+03	2.34e+01	56.0	5.43e-04
	16	1405	1405	1.42e+01	1.56e+01	4.96e-01	1.39	4.36e-11
	32	349	349	1.60e+01	1.40e+02	4.60e-01	3.74	5.20e-12

TABLE 1. Timing, memory and error results for applying the adaptive technique to each of the experiments in section 4.1 with different orders of discretization n_c .

4.2. Helmholtz problems. This section illustrates the performance of the discretization techniques when applied two Helmholtz problems of the form

$$-\Delta u - \omega^2 c(\mathbf{x})u = f(x, y)$$

on a square geometry Ω with an incident wave boundary condition $u(\mathbf{x}) = e^{i\omega \mathbf{d} \cdot \mathbf{x}}$ where $\mathbf{d} = (1, 0)$.

Two choices of geometry, coefficient function $c(\mathbf{x}) = c(x, y)$ and body load $f(x, y)$ are considered: *Constant coefficient:* For this experiment, $\Omega = (-1, 1)^2$ is twenty wavelengths in size ($\omega = 20\pi$),

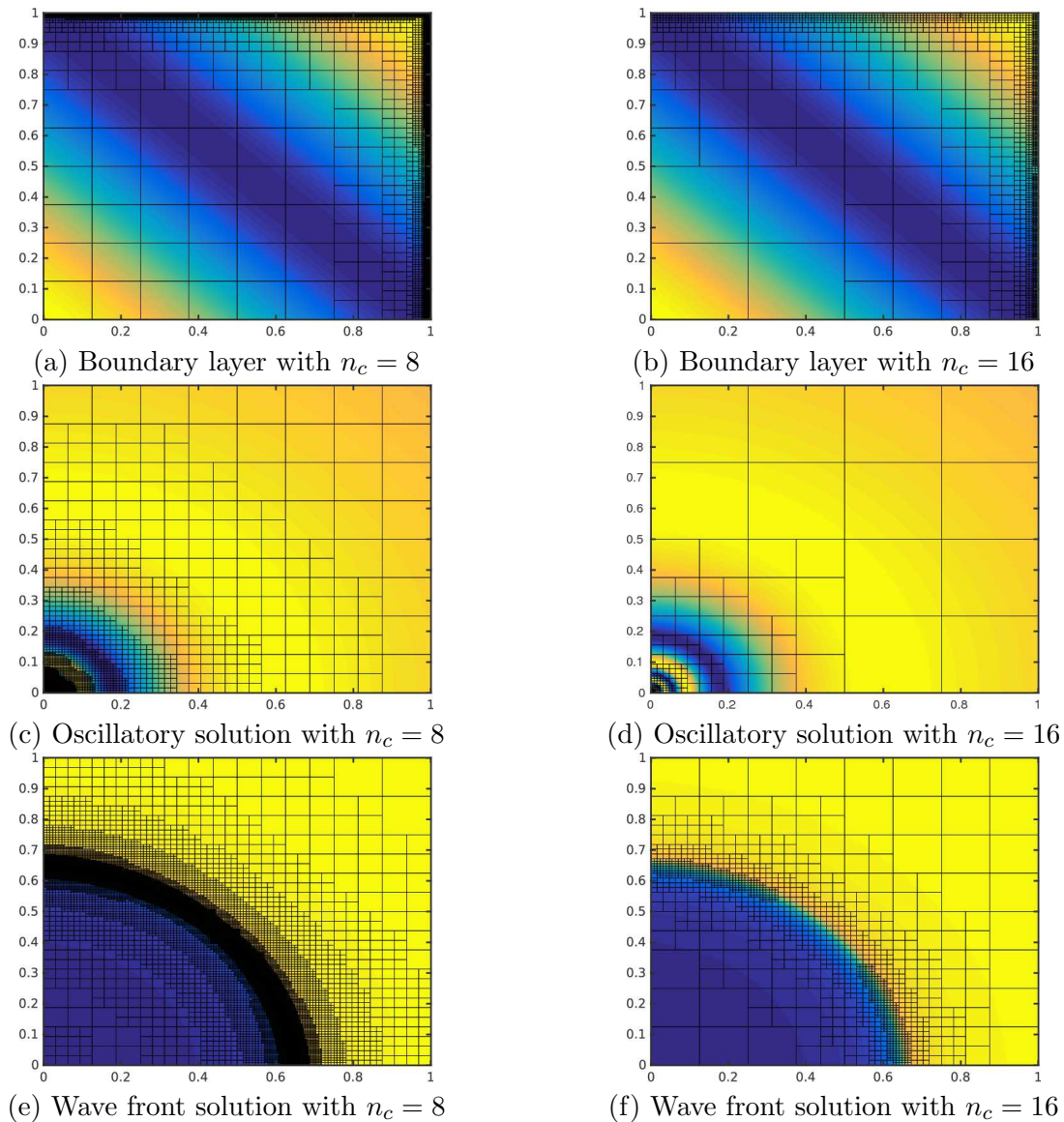


FIGURE 8. Illustration of the mesh generated by the adaptive discretization technique (overlaid on the solution) with $n_c = 8$ and 16 for the problems in section 4.1.

$c(\mathbf{x}) = 1$ and

$$f(x, y) = \frac{1}{\sqrt{2\pi} \cdot 0.005} e^{-\frac{x^2 + (y - 0.875)^2}{2(0.005)^2}}.$$

Variable medium: For this experiment, $\Omega = (-0.5, 0.5)^2$, $\omega = 150$, $f(\mathbf{x}) = 0$, and

$$c(\mathbf{x}) = c(x, y) = 4(y - 0.2)[1 - \operatorname{erf}(25(|\mathbf{x}| - 0.3))].$$

Figure 9 illustrates the real part of the solutions to these problems. A reference solution generated by applying the uniform discretization scheme until the relative convergence error was less than the stopping tolerance ϵ was used to generate the reference solution.

Table 5 reports on the performance of the adaptive discretization technique applied to the Helmholtz problems. Figure 10 illustrates the mesh resulting from the adaptive procedure. For

n_c	N_f	T_{pre}	T_s	R	E_{rel}
16	4	9.84e-02	4.07e-02	0.003	9.46e-01
	16	2.14e-01	2.01e-02	0.01	2.63e-01
	64	4.39e-01	2.95e-02	0.06	4.21e-02
	256	1.40e+00	1.24e-01	0.24	2.19e-03
	1024	5.83e+00	5.45e-01	1.05	2.79e-05
	4096	2.49e+01	3.93e+00	4.52	5.40e-08
	16384	1.19e+02	1.76e+01	19.3	1.93e-11
32	4	3.69e-01	3.93e-02	0.04	7.92e-02
	16	1.21e+00	3.61e-02	0.16	5.15e-03
	64	3.89e+00	1.32e-01	0.67	4.72e-05
	256	1.51e+01	1.60e+00	2.76	1.74e-08
	1024	1.01e+02	6.36e+00	11.4	1.22e-13

TABLE 2. Timing, memory and error results for applying the uniform discretization technique to the boundary layer problem with different orders of discretization n_c .

n_c	N_f	T_{pre}	T_s	R	E_{rel}
16	4	1.25e-01	2.79e-02	0.003	4.78e-01
	16	2.20e-01	1.82e-02	0.01	6.44e-01
	64	5.12e-01	3.39e-02	0.06	5.97e-01
	256	1.63e+00	9.50e-02	0.24	1.11e-01
	1024	6.03e+00	3.78e-01	1.05	6.16e-04
	4096	2.32e+01	2.52e+00	4.52	2.55e-05
	16384	1.00e+02	1.50e+01	19.3	3.25e-06
	65536	4.27e+02	6.51e+01	82.4	4.09e-07
32	4	4.05e-01	3.57e-02	0.04	4.88e-01
	16	1.07e+00	3.61e-02	0.16	6.93e-03
	64	3.27e+00	7.04e-02	0.67	5.35e-04
	256	1.41e+01	3.06e+00	2.76	1.64e-05
	1024	5.65e+01	1.30e+01	11.4	2.24e-06
	4096	2.34e+02	4.73e+01	47.0	3.10e-07
	16384	1.00e+03	1.68e+02	194.0	4.36e-08

TABLE 3. Timing, memory and error results for applying the uniform discretization technique to the locally oscillatory problem with different orders of discretization n_c .

the constant coefficient case, the Gaussian body load is not located close to the $n_c = 8$ discretization points on $\Omega^1 = \Omega$, thus the adaptive procedure was not able to capture it. To rectify this, we started the adaptive procedure with an initialized 16×16 uniform mesh. Since high order discretization techniques are better suited for high frequency problems, we only consider $n_c = 16$ and $n_c = 32$ for the variable coefficient problem. The results for both problems indicate there is no benefit in running the adaptive discretization technique with a really high order discretization ($n_c = 32$). The choice of $n_c = 16$ is faster in the precomputation plus the solve time and memory are comparable.

Tables 6 and 7 report on the performance of the uniform HPS discretization for the constant coefficient and variable coefficient problems, respectively, with $n_c = 16$ and 32. Notice that the adaptive method not only requires a smaller number of discretization points, it is also faster for both the precomputation and apply stages than the uniform method to achieve the same accuracy.

n_c	N_f	T_{pre}	T_s	R	E_{rel}
16	4	1.52e-01	3.35e-02	0.003	1.24e-01
	16	3.73e-01	1.97e-02	0.01	5.50e-03
	64	9.55e-01	1.94e-02	0.06	1.08e-04
	256	3.85e+00	7.24e-02	0.24	1.95e-06
	1024	1.47e+01	4.40e-01	1.05	1.93e-09
	4096	4.83e+01	2.21e+00	4.52	1.84e-11
32	4	8.79e-01	3.61e-02	0.04	3.20e-03
	16	1.12e+00	2.72e-02	0.16	9.22e-05
	64	3.75e+00	2.14e-01	0.67	8.69e-08
	256	1.49e+01	2.46e+00	2.76	2.07e-11
	1024	5.65e+01	1.33e+01	11.4	1.66e-11
	4096	2.30e+02	4.78e+01	47.0	6.71e-11

TABLE 4. Timing, memory and error results for applying the uniform discretization technique to the wave front problem with different orders of discretization n_c .

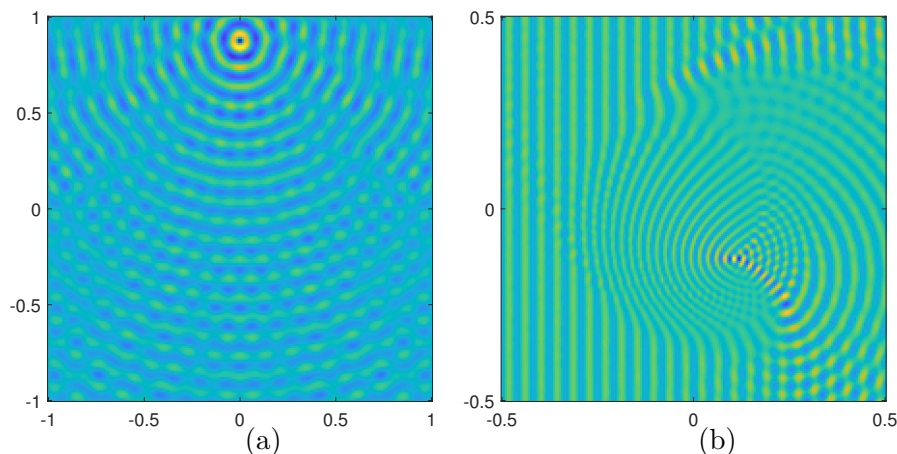


FIGURE 9. Illustration of the real part of the solutions to the problems under consideration in section 4.2: (a) constant coefficient and (b) variable coefficient.

Problem	n_c	N_i	N_f	T_i	T_f	T_s	R	E_{rel}
Constant	8	1576	14470	2.54e+00	3.04e+02	2.91e+00	5.242	1.02e-05
	16	1	460	4.09e-02	1.71e+01	2.44e-01	1.081	8.06e-06
	32	1	64	1.68e-01	3.45e+01	1.31e-01	1.504	9.33e-07
Variable	16	64	610	7.37e-01	2.06e+01	3.10e-01	1.434	4.60e-06
	32	16	61	2.71e+00	4.31e+01	1.54e-01	1.431	1.06e-05

TABLE 5. Timing, memory and error results for applying the adaptive technique to the Helmholtz problems in section 4.2.

5. CONCLUDING REMARKS

This manuscript presents an high order adaptive discretization technique that comes with an efficient direct solver. The HPS method presented here uses a *new* local pseudospectral discretization that does not involve corner points. By removing the corner points, the leaf computations are less expensive and more stable than the previous version of the method.

The adaptive discretization technique utilizes the modified local tensor product basis to look at convergence of the directional Chebyshev expansions to determine which regions of the domain

n_c	N_f	T_f	T_s	R	E_{rel}
16	4	1.43e-01	2.30e-02	0.007	2.50e-01
	16	4.23e-01	4.25e-02	0.031	7.02e+00
	64	1.31e+00	3.33e-02	0.136	2.21e-01
	256	5.13e+00	1.09e-01	0.591	1.40e-03
	1024	2.00e+01	5.13e-01	2.554	1.20e-04
	4096	7.75e+01	6.73e+00	10.98	2.02e-06
	16384	3.12e+02	3.57e+01	46.98	1.91e-09
32	4	1.09e+00	3.14e-02	0.087	5.35e-01
	16	3.71e+00	8.50e-02	0.362	1.04e-01
	64	1.40e+01	3.07e-01	1.505	2.75e-02
	256	5.61e+01	3.23e+00	6.238	2.20e-07
	1024	2.35e+02	1.84e+01	25.83	4.05e-09

TABLE 6. Timing, memory and error results solving the constant coefficient Helmholtz problem in section 4.2 with a uniform discretization.

n_c	N_f	T_f	T_s	R	E_{ref}
16	4	1.69e-01	2.34e-02	0.007	2.35e-01
	16	5.00e-01	1.58e-02	0.031	2.89e-01
	64	1.49e+00	2.63e-02	0.136	1.89e-01
	256	5.91e+00	1.01e-01	0.591	7.76e-04
	1024	2.43e+01	8.95e-01	2.554	7.47e-08
	4096	9.04e+01	8.98e+00	10.98	1.24e-10
	16384	3.21e+02	3.77e+01	46.98	7.78e-10
32	4	1.21e+00	3.20e-02	0.087	2.64e-01
	16	4.45e+00	3.67e-02	0.362	1.54e-01
	64	1.63e+01	2.85e-01	1.505	2.29e-06
	256	6.19e+01	3.72e+00	6.238	9.24e-11
	1024	2.76e+02	1.71e+01	25.83	6.23e-10

TABLE 7. Timing, memory and error results solving the variable coefficient Helmholtz problem in section 4.2 with a uniform discretization.

Ω need refinement. Since a discretization is based on decomposing the domain, updating the accompanying direct solver after refinement is inexpensive. The numerical results show that method is able to achieve the user prescribed accuracy and refines only of regions where it is necessary. For all problems the cost of applying and storing the direct solver resulting from the adaptive discretization technique is less than using a uniform discretization. For problems where the solution is globally oscillatory the cost of adaptive discretization technique is less than a uniform discretization.

6. ACKNOWLEDGEMENTS

The work by A. Gillman is supported by the Alfred P. Sloan foundation and the National Science Foundation (DMS-1522631). The work by P. Geldermans is supported by the National Science Foundation Graduate Research Fellowship under Grant No. 1450681.

REFERENCES

- [1] T. Babb, A. Gillman, S. Hao, and P.G. Martinsson, An accelerated Poisson solver based on a multidomain spectral discretization, In review.

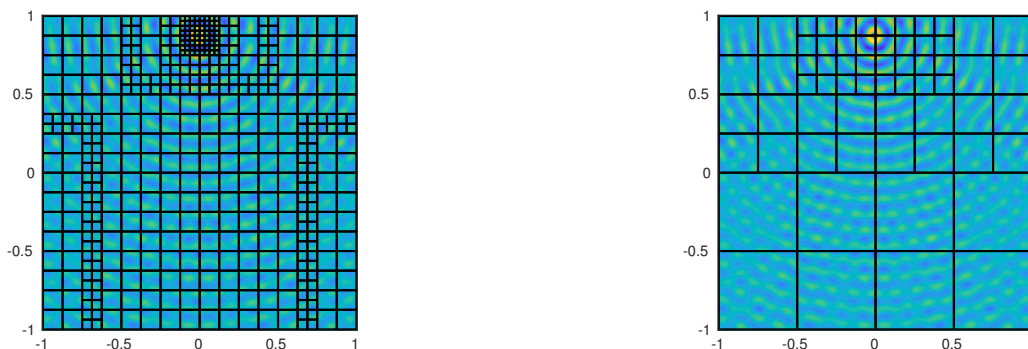
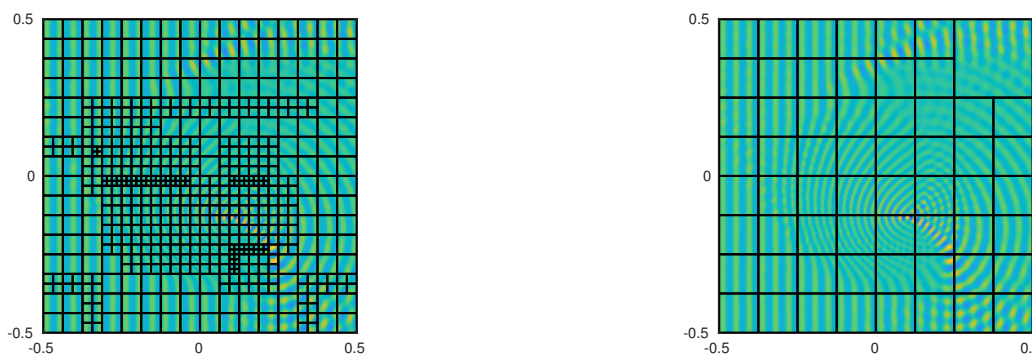
(a) Constant coefficient with $n_c = 16$ (b) Constant coefficient with $n_c = 32$ (c) Variable coefficient with $n_c = 16$ (d) Variable coefficient with $n_c = 32$

FIGURE 10. Illustration of the mesh generated by the adaptive discretization technique (overlayed on the solution) with $n_c = 16$ and $n_c = 32$ for the Helmholtz problems considered in section 4.2.

- [2] I. Babuvka and W. Rheinboldt, Error Estimates for Adaptive Finite Element Computations, SIAM Journal on Numerical Analysis, **15** (1978), no. 4, 736–754.
- [3] I. Babuka, F. Ihlenburg, T. Strouboulis, and S. K. Gangaraj, A posteriori error estimation for finite element solutions of Helmholtz equation. part I: the quality of local indicators and estimators, International Journal for Numerical Methods in Engineering, **40** (1997), 3443–3462.
- [4] A. Bayliss, C. I. Goldstein, and E. Turkel, The numerical solution of the Helmholtz equation for wave propagation problems in underwater acoustics, Computers and Mathematics with Applications, **11** (1985), 655–665.
- [5] C. Borges, A. Gillman, and L. Greengard, High resolution inverse scattering in two dimensions using recursive linearization, SIAM Journal of Imaging Sciences, **10** (2017), no. 2, 641–664.
- [6] C. Borges, and G. Biros, Reconstruction of a compactly supported sound profile in the presence of a random background medium (In review), <https://arxiv.org/abs/1805.01980>.
- [7] J. Boyd, Chebyshev and fourier spectral methods, Dover, 2000.
- [8] C. Carstensen and R. H. W. Hoppe, Error Reduction and Convergence for an Adaptive Mixed Finite Element Method, Mathematics of Computation, **75** (2006), no. 255, 1033–1042.
- [9] Y. Chen, Recursive Linearization for Inverse Scattering, Yale Research Report/DCS/RR-1088, 1995.
- [10] L. Demkowicz, Computing with Hp-Adaptive Finite Elements, Vol. 1: One and Two Dimensional Elliptic and Maxwell Problems, Chapman and Hall, 2006.
- [11] L. Demkowicz, J. Kurtz, D. Pardo, M. Paszynski, W. Rachowicz, and A. Zdunek, Computing with Hp-Adaptive Finite Elements, Vol. 2: Frontiers: Three Dimensional Elliptic and Maxwell Problems with Applications, Chapman and Hall, 2007.
- [12] I.S. Duff, A.M. Erisman, and J.K. Reid, Direct methods for sparse matrices, Oxford, 1989.
- [13] K. Eriksson and C. Johnson, An adaptive finite element method for linear elliptic problems, Mathematics of Computation, **50**, (1988), 361–383.

- [14] Q. Fang, P. M. Meaney, and K. D. Paulsen, Viable Three-Dimensional Medical Microwave Tomography: Theory and Numerical Experiments, IEEE Transactions on Antennas and Propagation, **58** (2010), no. 2, 449–458.
- [15] A. George, Nested dissection of a regular finite element mesh, SIAM Journal on Numerical Analysis **10** (1973), 345–363.
- [16] A. Gillman, Fast direct solvers for elliptic partial differential equations, Ph.D. thesis, University of Colorado at Boulder, Applied Mathematics, 2011.
- [17] A. Gillman, A. Barnett, and P.G. Martinsson, A spectrally accurate direct solution technique for frequency-domain scattering problems with variable media, BIT Numerical Mathematics **55** (2015), no. 1, 141–170.
- [18] A. Gillman and P. Martinsson, A direct solver with $O(N)$ complexity for variable coefficient elliptic pdes discretized via a high-order composite spectral collocation method, SIAM Journal on Scientific Computing **36** (2014), no. 4, A2023–A2046.
- [19] A. J. Hoffman, M. S. Martin, and D. J. Rose, Complexity bounds for regular finite difference and finite element grids, SIAM J. Numer. Anal. **10** (1973), 364–369.
- [20] S. Le Borne, L. Grasedyck, and R. Kriemann, Domain-decomposition based \mathcal{H} -LU preconditioners, Domain decomposition methods in science and engineering XVI, Lecture Notes Computing Science in Engineering, vol. 55, Springer, Berlin, 2007, pp. 667–674.
- [21] J.Y. Lee and L. Greengard, A fast adaptive numerical method for stiff two-point boundary value problems, SIAM Journal of Scientific Computing **18** (1997), no. 2, 403–429.
- [22] P.G. Martinsson, A fast direct solver for a class of elliptic partial differential equations, Journal of Scientific Computing **38** (2009), no. 3, 316–330.
- [23] P.G. Martinsson, A direct solver for variable coefficient elliptic pdes discretized via a composite spectral collocation method, Journal of Computational Physics **242** (2013), no. 0, 460 – 479.
- [24] W. F. Mitchell, A collection of 2d elliptic problems for testing adaptive grid refinement algorithms, Applied Mathematics and Computation **220** (2013), 350 – 364.
- [25] P. Morin, R. Nocketto and K. Siebert, Convergence of Adaptive Finite Element Methods, SIAM Review, **44** (2002), no. 4, 631–658.
- [26] W. Rachowicz and L. Demkowicz, An hp-adaptive finite element method for electromagnetics: Part 1: Data structure and constrained approximation, Computer Methods in Applied Mechanics and Engineering, **187** (2000), 307 – 335.
- [27] P.G. Schmitz and L. Ying, A fast direct solver for elliptic problems on general meshes in 2d, Journal of Computational Physics **231** (2012), no. 4, 1314 – 1338.
- [28] S. Smith, Lebesgue constants in polynomial interpolation, Annales Mathematicae et Informaticae **33** (2006), 109–123.
- [29] L.N. Trefethen, Spectral methods in matlab, SIAM, Philadelphia, 2000.
- [30] , E. Wadbro, and M. Berggren, High Contrast Microwave Tomography using Topology Optimization Techniques, Journal of Computational and Applied Mathematics, **234** (2010), 1773–1780.
- [31] S. Wang, M. V. de Hoop, and J. Xia, On 3D modeling of seismic wave propagation via a structured parallel multifrontal direct Helmholtz solver, Geophysical Prospecting, **59** (2011), no. 5, 857–873.
- [32] E. L. Wilson, The static condensation algorithm, International Journal for Numerical Methods in Engineering **8** (1974), no. 1, 198–203.
- [33] J. Xia, S. Chandrasekaran, M. Gu, and X. S. Li, Superfast multifrontal method for large structured linear systems of equations, SIAM Journal of Matrix Analysis and Applications **31** (2009), no. 3, 1382–1411.

7. APPENDIX

Consider the variable coefficient Helmholtz impedance boundary value problem

$$(9) \quad \begin{aligned} -\Delta u - \omega^2 c(\mathbf{x})u &= s(x, y) & \mathbf{x} \in \Omega \\ \frac{\partial u}{\partial \nu} + i\eta u &= t(x, y) & \mathbf{x} \in \partial\Omega = \Gamma. \end{aligned}$$

where ν denotes the outward facing normal vector, $c(\mathbf{x})$ is a smooth function, $\omega \in \mathbb{R}$, and $\eta \in \mathbb{C}$.

This section presents the technique for solving variable coefficient Helmholtz problems such as (9) using the HPS method. This technique uses impedance-to-impedance (ItI) operators instead of the DtN operators used in the body of the paper.

Definition 7.1 (impedance-to-impedance map). Fix $\eta \in \mathbb{C}$, and $\mathcal{R} \setminus \eta \neq 0$. Let

$$(10) \quad f := u_n + i\eta u|_{\Gamma}$$

$$(11) \quad g := u_n - i\eta u|_{\Gamma}$$

be Robin traces of u . We refer to f and g as the “incoming” and “outgoing” (respectively) impedance data. For any $\omega > 0$, the *ItI operator* $R : L^2(\Gamma) \rightarrow L^2(\Gamma)$ is defined by

$$(12) \quad Rf = g$$

for f and g the Robin traces of u the solution of (9), for all $f \in L^2(\Gamma)$.

To make the solution technique useful for different choices of $s(x, y)$, we choose to represent the solution u as a superposition of the homogeneous solution w and the particular solution z ; i.e. $u = w + z$ where z is the solution of the following boundary value problem

$$\begin{aligned} -\Delta z - \omega^2 c(\mathbf{x})z &= s(x, y) & \mathbf{x} \in \Omega \\ \frac{\partial z}{\partial \nu} + i\eta z &= 0 & \mathbf{x} \in \partial\Omega = \Gamma \end{aligned}$$

and w is the solution of

$$\begin{aligned} -\Delta w - \omega^2 c(\mathbf{x})w &= 0 & \mathbf{x} \in \Omega \\ \frac{\partial w}{\partial \nu} + i\eta w &= t(x, y) & \mathbf{x} \in \partial\Omega = \Gamma. \end{aligned}$$

Section 7.1 presents the leaf computation and section 7.2 presents the technique for merging two boxes. Throughout the notation is kept consistent with that of section 2. When there is no body load (i.e. $s(x, y) = 0$), the method from [17] is recovered.

7.1. Leaf computation. This section presents the construction of the homogeneous and particular solutions to (9) using the modified spectral collocation method from section 2.1. Additionally, a matrix \mathbf{R} approximating the ItI operator for the homogeneous boundary value problem and the impedance boundary data generated by the particular solution are constructed.

Let \mathbf{N} denote the matrix that takes normal derivatives of the basis functions. Then \mathbf{N} is given by

$$\mathbf{N} = \begin{bmatrix} -\mathbf{D}_x(I_s, I^T) \\ \mathbf{D}_y(I_e, I^T) \\ \mathbf{D}_x(I_n, I^T) \\ -\mathbf{D}_y(I_w, I^T) \end{bmatrix}.$$

Then the matrix for creating the incoming impedance data is

$$\mathbf{F} = \mathbf{N} + i\eta \mathbf{I}_{n_c^2}(I_b, I^T)$$

and the matrix for creating the outgoing impedance data is

$$\mathbf{G} = \mathbf{N} - i\eta \mathbf{I}_{n_c^2}(I_b, I^T)$$

where $\mathbf{I}_{n_c^2}$ is the identity matrix of size n_c^2 .

Then the discretized body load problem to find the approximation to z at the collocation points takes the form

$$(13) \quad \mathbf{B} \begin{bmatrix} \mathbf{z}_b \\ \mathbf{z}_i \end{bmatrix} = \begin{bmatrix} \mathbf{F} \\ \mathbf{A}(i, b) \ \mathbf{A}(i, i) \end{bmatrix} \mathbf{z} = \begin{bmatrix} \mathbf{0} \\ \mathbf{s} \end{bmatrix}$$

where \mathbf{z} is the vector with the approximate values of z at the collocation points, and \mathbf{s} is $s(x, y)$ evaluated at the interior points.

So the solution operator \mathbf{Y} which gives the approximate particular solution is the solution to

$$\mathbf{B}\mathbf{Y} = \begin{bmatrix} \mathbf{0}_{4n_c-4 \times (n_c-2)^2} \\ \mathbf{I}_{(n_c-2)^2} \end{bmatrix}.$$

Likewise the solution operator $\mathbf{\Psi}$ which give the approximate solution to the homogeneous problem is the solution to

$$\mathbf{B}\mathbf{\Psi} = \begin{bmatrix} \mathbf{I}_{4n_c-4} \\ \mathbf{0}_{(n_c-2)^2 \times 4n_c-4} \end{bmatrix}.$$

To construct the outgoing impedance data from the particular solution \mathbf{h} , the matrix \mathbf{G} needs to be applied to the solution of (13); i.e.

$$\mathbf{h} = \mathbf{G}\mathbf{Y} \begin{bmatrix} \mathbf{0} \\ \mathbf{s} \end{bmatrix} = \mathbf{W} \begin{bmatrix} \mathbf{0} \\ \mathbf{s} \end{bmatrix}.$$

The approximate ItI operator is constructed in the same manner as in [17]. That is

$$\mathbf{R} = \mathbf{G}\mathbf{\Psi}.$$

Putting these together, we find that the outgoing impedance data from the box is given by

$$\mathbf{g} = \mathbf{R}\mathbf{t} + \mathbf{h}$$

where \mathbf{t} is the evaluation of the incoming boundary data function $t(x, y)$ at the points on the boundary.

7.2. Merge two boxes. This section presents the technique for merging two boxes $\Omega^\tau = \Omega^\alpha \cup \Omega^\beta$ for which the ItI matrices and outgoing impedance data from the particular solution has already been computed. In other words, the matrices \mathbf{R}^α and \mathbf{R}^β along with the vectors \mathbf{h}^α and \mathbf{h}^β are available. For consistency, we used the same notation as in [17]. In this section, it is important to remember that the unlike the DtN version of the algorithm, the normal derivatives are always pointing exterior to the region they are defined on.

Using the same ordering as in section 2.2, the outgoing impedance data for boxes α and β are given by

$$\begin{bmatrix} \mathbf{g}_1^\alpha \\ \mathbf{g}_3^\alpha \end{bmatrix} = \begin{bmatrix} \mathbf{R}_{11}^\alpha & \mathbf{R}_{13}^\alpha \\ \mathbf{R}_{31}^\alpha & \mathbf{R}_{33}^\alpha \end{bmatrix} \begin{bmatrix} \mathbf{t}_1^\alpha \\ \mathbf{t}_3^\alpha \end{bmatrix} + \begin{bmatrix} \mathbf{h}_1^\alpha \\ \mathbf{h}_3^\alpha \end{bmatrix}; \quad \begin{bmatrix} \mathbf{g}_2^\beta \\ \mathbf{g}_3^\beta \end{bmatrix} = \begin{bmatrix} \mathbf{R}_{22}^\beta & \mathbf{R}_{23}^\beta \\ \mathbf{R}_{32}^\beta & \mathbf{R}_{33}^\beta \end{bmatrix} \begin{bmatrix} \mathbf{t}_2^\beta \\ \mathbf{t}_3^\beta \end{bmatrix} + \begin{bmatrix} \mathbf{h}_2^\beta \\ \mathbf{h}_3^\beta \end{bmatrix}$$

where $\begin{bmatrix} \mathbf{h}_1^\alpha \\ \mathbf{h}_3^\alpha \end{bmatrix}$ and $\begin{bmatrix} \mathbf{h}_2^\beta \\ \mathbf{h}_3^\beta \end{bmatrix}$ are the outgoing impedance data due to the particular solutions on each box.

Since the normal vectors are opposite in each box, we know $\mathbf{t}_3^\alpha = -\mathbf{g}_3^\beta$ and $\mathbf{g}_3^\alpha = -\mathbf{t}_3^\beta$. Using this information in the bottom row equations, \mathbf{t}_3^α and \mathbf{t}_3^β can found in terms of \mathbf{t}_1^α , \mathbf{t}_2^β , \mathbf{h}_3^α , and \mathbf{h}_3^β . They are given by

$$(14) \quad \mathbf{t}_3^\alpha = \mathbf{W}^{-1} \left[\mathbf{R}_{33}^\beta \mathbf{R}_{31}^\alpha - \mathbf{R}_{32}^\beta \right] \begin{bmatrix} \mathbf{t}_1^\alpha \\ \mathbf{t}_2^\beta \end{bmatrix} + \mathbf{W}^{-1} \left(\mathbf{R}_{33}^\beta \mathbf{h}_3^\alpha - \mathbf{h}_3^\beta \right)$$

and

$$(15) \quad \mathbf{t}_3^\beta = \left[-\mathbf{R}_{31}^\alpha - \mathbf{R}_{33}^\alpha \mathbf{W}^{-1} \mathbf{R}_{33}^\beta \mathbf{R}_{31}^\alpha \mid \mathbf{R}_{33}^\alpha \mathbf{W}^{-1} \mathbf{R}_{32}^\beta \right] \begin{bmatrix} \mathbf{t}_1^\alpha \\ \mathbf{t}_2^\beta \end{bmatrix} - \left(\mathbf{I} + \mathbf{R}_{33}^\alpha \mathbf{W}^{-1} \mathbf{R}_{33}^\beta \right) \mathbf{h}_3^\alpha + \mathbf{R}_{33}^\alpha \mathbf{W}^{-1} \mathbf{h}_3^\beta$$

where $\mathbf{W} = \mathbf{I} - \mathbf{R}_{33}^\beta \mathbf{R}_{33}^\alpha$.

Plugging (14) and (15) into the top row equations results in the following expression for the outgoing impedance data for the box $\Omega^\alpha \cup \Omega^\beta$

$$\begin{aligned}
(16) \quad \begin{bmatrix} \mathbf{g}_1^\alpha \\ \mathbf{g}_2^\beta \end{bmatrix} &= \begin{bmatrix} \mathbf{R}_{11}^\alpha + \mathbf{R}_{13}^\alpha \mathbf{W}^{-1} \mathbf{R}_{33}^\beta \mathbf{R}_{31}^\alpha & -\mathbf{R}_{13}^\alpha \mathbf{W}^{-1} \mathbf{R}_{32}^\beta \\ -\mathbf{R}_{23}^\beta \left(\mathbf{R}_{31}^\alpha + \mathbf{R}_{33}^\alpha \mathbf{W}^{-1} \mathbf{R}_{33}^\beta \mathbf{R}_{31}^\alpha \right) & \mathbf{R}_{22}^\beta + \mathbf{R}_{23}^\beta \mathbf{R}_{33}^\alpha \mathbf{W}^{-1} \mathbf{R}_{32}^\beta \end{bmatrix} \begin{bmatrix} \mathbf{t}_1^\alpha \\ \mathbf{t}_2^\beta \end{bmatrix} \\
&+ \begin{bmatrix} \mathbf{h}_1^\alpha \\ \mathbf{h}_2^\beta \end{bmatrix} + \begin{bmatrix} \mathbf{R}_{13}^\alpha \mathbf{W}^{-1} \left(\mathbf{R}_{33}^\alpha \mathbf{h}_3^\alpha - \mathbf{h}_3^\beta \right) \\ -\mathbf{R}_{23}^\beta \left(\mathbf{I} + \mathbf{R}_{33}^\alpha \mathbf{W}^{-1} \mathbf{R}_{33}^\beta \right) \mathbf{h}_3^\alpha + \mathbf{R}_{23}^\beta \mathbf{R}_{33}^\alpha \mathbf{W}^{-1} \mathbf{h}_3^\beta \end{bmatrix} \\
&= \mathbf{R}^\tau \begin{bmatrix} \mathbf{t}_1^\alpha \\ \mathbf{t}_2^\beta \end{bmatrix} + \begin{bmatrix} \hat{\mathbf{h}}_1^\alpha \\ \hat{\mathbf{h}}_2^\beta \end{bmatrix}
\end{aligned}$$

7.3. The full algorithm. As with the homogeneous DtN solution technique, the solver can be broken into the precomputation and the solve phase. The precomputation for a leaf box τ is similar to before except now a solution operator \mathbf{Y}^τ yielding the particular solution on τ and a matrix \mathbf{W} giving the outgoing particular impedance data are constructed. Also, instead of a DtN matrix, an ItI matrix is constructed. The precomputation for a box τ with children α and β is more intense. A collection of operators giving the incoming impedance data on the shared edge are constructed from the incoming impedance data from τ and the outgoing impedance particular solution data (which is not yet computed) on that edge from both α and β . Thus a collection of operators for constructing the outgoing particular solution on the shared edge are constructed as well as the operators needed to construct the outgoing impedance particular solution data on the boundary of τ . Notice looking the formulas (14), (15) and (16) there is significant overlap in computation thus keeping the cost and memory of the precomputation in check.

The solve step sweeps the tree twice (instead of once as in the homogeneous solver). First, starting from the leaf boxes moving up the tree to Ω^1 , the outgoing impedance particular solution data are constructed. Then using this information along with the boundary condition on Ω , the incoming impedance boundary data is propagated from the top of the tree down to the leaf boxes.